Proceedings of the ASME 2024
Fluids Engineering Division Summer Meeting
FEDSM2024
July 15-17, 2024, Anaheim, CA

FEDSM2024-131545

PIV AND HIGH-SPEED IMAGING INVESTIGATION OF FALLING LIQUID DROPLET PROPERTIES

Noushin Azimy*[1], Emmelia Lichty[2], Keldon Anderson[1], Soroor Karimi[1]

[1]Department of Mechanical Engineering
University of Tulsa, Tulsa, OK, USA
[2]Department of Mechanical Engineering
Oral Roberts University, Tulsa, OK, USA

ABSTRACT

Liquid droplet impact is a subject that has been investigated in both engineering and non-engineering applications to understand and to control this phenomenon. Spray cooling, ink-jet printing, spray coating and painting, soil erosion prevention, pesticide application, and impact erosion are merely a few examples in which droplet impact is involved. Erosion caused by droplet impact on a solid surface is important in numerous elements of industrial equipment, such as pipelines, steam turbines, and wind turbine blades. Though experimental and modeling studies have been performed on this topic, most failed to perform quantitative investigation especially when it came to the erosion of wind turbine blades. Moreover, most approaches assume that the impacting droplets are completely spherical and unaffected by any local turbulence or vortex shedding. As the droplet erosion process could be affected by several parameters, such as the impact velocity, shape and size of the droplets, this study focuses on investigating droplet properties and movement in a controlled lab environment. High speed imaging and Particle Image Velocimetry (PIV) methods are used for this purpose. PIV is used to measure the velocity, circularity, and size of the falling droplets in both disturbed and un-disturbed flow conditions. High-speed camera imaging provides additional insight to the path of the droplets' movement in the presence of any turbulence. Experiments are performed at a variety of flow rates utilizing a range of blunt needle gauge sizes to create different droplet sizes. It is observed that the blunt needles produce a train of droplets that are different in size following each leading droplet. This is a crucial observation as it will have a direct impact on the magnitude of erosion and should be considered in the future modeling efforts.

Keywords: Particle image velocimetry, liquid droplets, high-speed imaging, droplet properties

* Corresponding author: noushin-azimy@utulsa.edu

NOMENCLATURE

A	Area of the shape of liquid droplets
P	Perimeter of the shape of liquid droplets
We	Weber number
Oh	Ohnesorge number
μ	Viscosity
ρ	Density
σ	Surface tension
D	Diameter
x	Variable
R	Mean
SD	Standard Deviation
N	Count

1. INTRODUCTION

Liquid droplet impact erosion is a design issue in the steam and wind turbine and aerospace industry, and it has performance hindrance characteristics with other damage sources like cavitation. The liquid droplets are influenced by different parameters such as velocity impingement, droplets' shape and size, and flow rate. Various studies are done to evaluate the effect of droplet impacts on surfaces and their properties. Hoksbergen et al. [1] discussed the contact pressure resulting from liquid droplet impact on (elastic) solid targets with and without air cushioning. The contact pressure is influenced by the velocity of the droplet or target and the presence of air cushioning. An analytical model and a numerical model were developed to study this phenomenon and it was found that the maximum pressure occurring during the impact event significantly changes when air cushioning is included. Moreover, the relation between the maximum contact pressure and the impact velocity was found to be quadratic. This has implications for interpreting experimental results which commonly define lifetime as a function of impact velocity instead of stress. The developed model can be used to model stress wave initiation and propagation in materials used

© 2024 by ASME

for wind turbine coatings, steam turbines, and aerospace. Liu et al. [2] investigated the high-speed dynamics and temperature variation during droplet impact on a heated surface. Their outcomes demonstrate that for non-Leidenfrost droplets, mean droplet temperature change (ΔTd) increases with increasing Weber number (We) and initial substrate temperature. Marzbali and Dolatabadi [3] examined the impact of water droplets on a dry rigid substrate and liquid films using a compressible VOF solver. Two new correlations were developed to estimate the maximum pressure generated by the impact of a single droplet onto dry and wetted surfaces. The simulations revealed the air entrapment and maximum pressure when lateral jetting occurs, and a linear correlation between non-dimensional maximum pressure and Mach number was developed for impact velocities between 100 m/s and 500 m/s. Additionally, the formation of low-pressure stripes due to reflection of the compression waves and the damping of the lateral jet formation were observed. Cimpeanu and Papageorgiou [4] presented a numerical framework to investigate three-dimensional drop impact at high velocities, providing a reliable local description of the flow in which a full interaction between the air and the liquid is permitted. Results show pre-impact deformation and break-up in agreement with available experiments in the relevant parameter range. Violent splashing is observed for drops over 50 μm in diameter, with topological changes such as droplet break-off or coalescence and potential re-impingement of smaller fragments. Variation in the angle of impingement reveals corner-type features at the advancing impact front, and the average number of secondary drops resulting from the impact increases with the initial droplet diameter. Tang et al. [5] systematically investigated the dynamics of droplet impact on cold and dry solid surfaces, focusing on the effect of surface roughness. High speed images showed that liquid droplets spread on the surface in the form of a rim-bounded lamella, except fuel droplets, which contract back after reaching the maximum spreading diameter. The non-dimensional spreading diameter (β) was found to increase with increasing Weber number (We) and Ohnesorge number (Oh), with β_{max} depending primarily on (We/Oh). The transition from spreading to splashing was characterized by a critical value of (We/Oh)1/2 and fitted empirically as a function of surface roughness. β_{max} and Oh number are defined as (Eqn. 1) and (Eqn. 2) [5]. μ (N·m^{-1}), ρ (g·cm^3), σ (N·m^{-1}), D_0 (mm), and D_{max} (mm) are viscosity, density, surface tension, diameter, and maximum spreading diameter of the droplet. Haller et al. [6] simulations showed that a high velocity droplet impacting a rigid target can generate a shock wave attached to the contact edge of the droplet. This shock wave travels along the droplet's free surface and is reflected into the bulk of the liquid as an expansion wave, leading to an eruption of intense lateral jetting.

$$Oh = \frac{\mu}{\rho \sigma D_0} \quad (1)$$

$$\beta_{max} = \frac{D_{max}}{D_0} \quad (2)$$

Different investigations have been done experimentally and numerically to measure the droplets properties and evaluate the impact of liquid droplets on surface damage [7, 8, 9, 10]. However, the majority of them have failed to do quantitative research, particularly on wind turbine blade erosion. In most of the investigations, the shape of droplets has been assumed spherical, and the turbulence effects were neglected. This study presents the properties and movement of liquid droplets in a lab environment in both disturbed and un-disturbed flow situation using high speed imaging and Particle Image Velocimetry (PIV) methods at different flow rates and different droplet sizes.

2. MATERIALS AND METHODS

2.1 Testing Materials

Previous work by Anderson et al. focused on investigating falling liquid droplet properties to produce a well-defined artificial rain field to be used for testing water droplet erosion on wind turbine blades [11]. Ahmad et al. [12] determined that impacting droplet diameter was one of the key parameters affecting droplet erosion. Natural rain droplet diameters vary in size from around 0.2 mm to 5 mm [13]. Therefore, an assortment of blunt needles with differing gauge numbers was selected to produce water droplets within this range. Figure 1 displays the selected sizes with their characteristics. A wide variety of needles coupled with an adjustable flow rate allows the facility to simulate and measure the liquid droplets for different rain intensities, and thus different severities of erosion.

FIGURE 1: SIZE COMPARISON OF NEEDLE GAUGES USED TO PRODUCE WATER DROPLETS.

2.2 Testing Apparatus

Figure 2 shows a general schematic of the two-dimensional, two component (2D-2C) Particle Image Velocimetry (PIV) system used in this study. The system components consist of a dual YAG laser, synchronizer, CCD camera, processor, and droplet source as shown in Figure 3. The laser has a wavelength of 532 nm, and the manufacturer is EverGreen. The synchronizer is the TSI LaserPulse Model 610036, and the camera is a TSI

© 2024 by ASME

Powerview Plus equipped with a Tokina AT-X MACRO 100 F2.8 D lens. The processor runs Insight4G Software that can determine a vast number of flow field measurements, with particle diameter, circularity, and velocity magnitude being the key properties in this study due to their effect on droplet erosion.

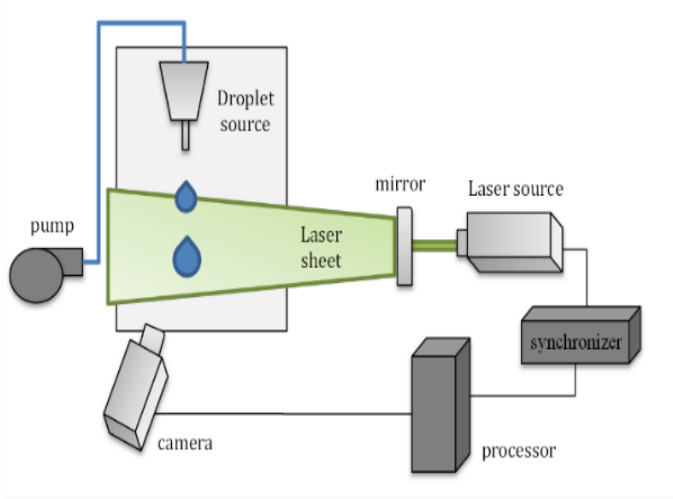

FIGURE 2: SCHEMATIC OF PIV SYSTEM USED.

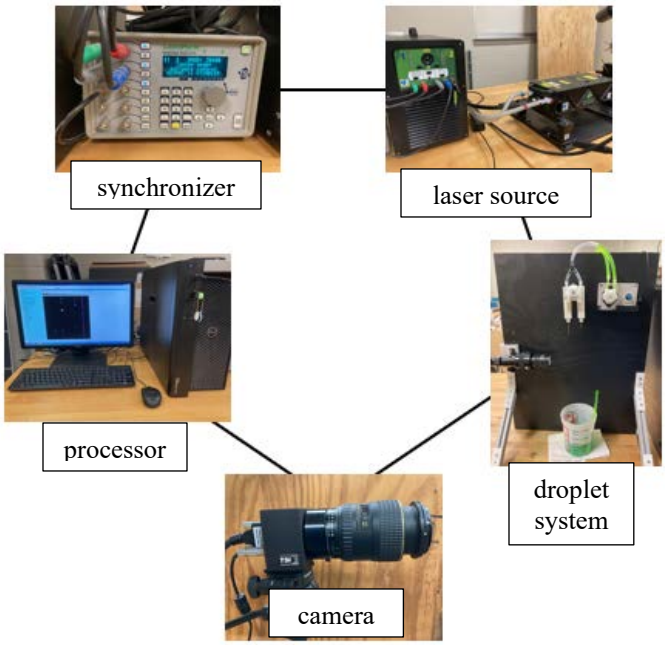

FIGURE 3: IMAGES OF PIV SYSTEM COMPONENTS.

Figure 4 displays the droplet source which is a wooden frame that houses the blower, laser head, and peristaltic pump. The blower is connected to the frame with adjustable location. It has various power settings and is equipped with a 3D printed shutter that changes the air outlet area and directs the air flow. The adjustable laser head is mounted to the frame to ensure the proper alignment of the laser sheet directly through the path of the falling droplets. The peristaltic pump can provide a variety of flow rates. The flow rate used is dependent upon the equipped needle's GA number and limited by both the minimum pressure required to produce a flow of water and the maximum pressure before water escapes and leaks from the needle's attachment point.

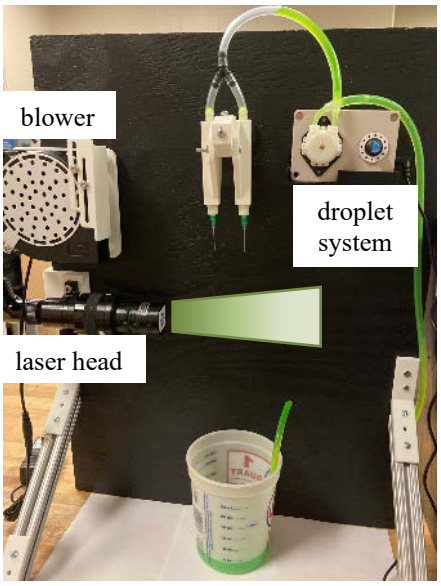

FIGURE 4: IMAGES OF WOODEN FRAME SUPPORTING LASER, BLOWER, DROPLET SOURCE, AND PUMP.

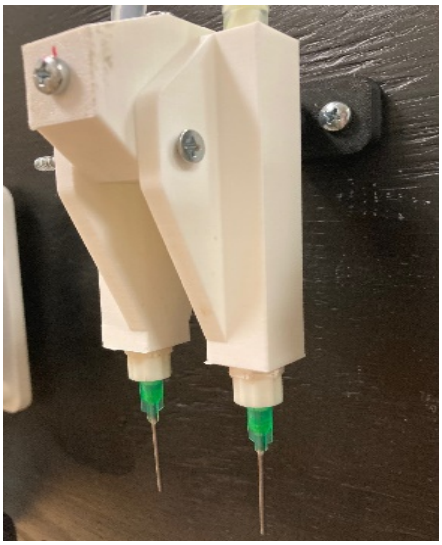

FIGURE 5: IMAGE OF 3D-PRINTED DROPLET SOURCE DEVICE WITH INTERCHANGEABLE BLUNT NEEDLES ATTACHED.

The droplet source consists of a 3D-printed device that holds the blunt needle and allows for the replacement of needles to form different droplet sizes. Figure 5 shows this closely with the 18 GA needles installed. Two devices equipped with blunt needles are in use at a time for the purpose of doubling the number of drops that are captured and analyzed in a single image. The working fluid, in a continuous cycle through the pump, is

© 2024 by ASME

tap water with a minimal amount of fluorescent dye added to reduce reflectivity while not changing further properties of the water. Approximately 3 mL of fluorescent dye was added per 150 mL of water. Without dye the images taken by the camera contain substantial glares due to the laser illumination and reflective nature of clear water. The minimum laser power needed to produce acceptable PIV images is also used for this reason. The glares render images useless by covering other water droplets in the PIV image and falsely expanding the size of the particles measured by the Insight4G software.

2.3 Experimental Method

Power is supplied to the processor, synchronizer, laser, and CCD camera, and the PIV software Insight4G is launched. Particle and timing settings are adjusted as recommended by the software manual. The CCD camera is properly focused and calibrated by using a reference object of known size in the frame to establish the pixels to millimeter ratio in the software.

The droplet source is started with the desired flow rate set and gauge needle installed. The flow is inspected and verified to be producing a steady stream of droplets from the tip of the blunt needle. The camera is turned to a low aperture with careful consideration to not change its position and all external light sources are removed to operate and adjust the laser. The laser alignment is checked to ensure it directly illuminates the path of the falling water droplets; the laser power, as well as the camera aperture, is adjusted to produce images with distinct water droplets, or particles, and few saturated pixels.

Once the camera, laser, and droplet source are properly running, the PIV sequence is started. The PIV system takes 250 sets of images where the two images within a set are taken 500μs apart to allow for the recommended distance to be traveled by the particle for calculating velocity with PIV. The images are verified to be of good quality with minimal glares and saturated pixels, and thus suitable for processing by Insight4G.

Within image processing, a mask can be imposed to constrain which region of particles in the image are processed. In this study the mask was drawn to contain the particles that had fallen the same distance the water droplets traveled before they contacted the specimen in the liquid droplet erosion testing facility [7]. The particle sizing settings are modified depending on the images to produce the most accurate processing results through lowering or raising the binarization threshold to better define the water particles from the black background. Increasing the sensitivity of the binarization also assists the software in defining several separate particles that are close together and in more accurately measuring droplets' size and shape. The minimum and maximum particle diameter recognized by the software is altered depending on the GA number of the blunt needle used. When setting the maximum particle size, careful consideration is made to ensure the inclusion of the largest drops produced by the needle, but not much larger is permitted to prevent the software from analyzing multiple droplets in close proximity as one larger particle.

Histograms displaying the count of particles for diameter, circularity, and velocity magnitude distributions are analyzed for the most frequently occurring number, or the mode. Additionally, a data file can be written from the histogram and analyzed in Excel or MATLAB to calculate the true average.

This process of PIV is repeated for static, or undisturbed, flow of the droplets for the array of needle sizes shown in Figure 1, as well as for disturbed flow of the droplets for some GA numbers utilizing the blower attached to the wooden frame shown in Figure 4. The disturbed flow simulates the turbulence caused by moving blades (arms) that the droplets will experience in the water droplet erosion facility. Images are taken of the water droplet's path of deflection within the facility, as well as the path produced by the droplet source and blower, and Adobe Photoshop is used to determine and ensure similar degrees of deflection from the vertical for the droplets. This is done by first taking images of the droplet's path from a level camera. An image is then opened in Adobe Photoshop and the Rectangular Marquee tool used to draw and measure a vertical rectangle encompassing the movement of the droplets. Using the width and height measured in pixels by Adobe and trigonometry, the angle of deflection from the vertical is calculated. The path of movement of the droplets is estimated to be 10-17 degrees from the vertical in the facility for droplets produced by the 15 GA blunt needle. The blower speed necessary to replicate this amount of deflection for a 15 GA blunt needle is measured using the anemometer directly below the needles and found to be approximately 3 m/s.

3. RESULTS AND DISCUSSION

The PIV system is able to evaluate liquid droplet falling properties such as velocity, droplets circularity, and diameter. The liquid used in this study is water at different flow rates ranging from 0.1 mL/s to 1.19 mL/s for both static and disturbed flow. Moreover, three needle sizes are used: 14 GA, 15 GA, and 18 GA.. The effects of changing the needle size on droplets diameter are shown in Figure 6. By increasing the nominal inner diameter of needles from 0.514 mm to 1.600 mm, the average leading droplets diameter is increased up to 3.50 mm. The PIV test takes a set number of images of droplets falling in order to examine their fluidic characteristics. Insight software records the velocity, diameter, and circularity of droplets from the images and exports the data to Tecplot. The data file for each parameter is imported into Excel software, where the standard deviation is determined using the Excel function. The standard deviation is defined by (Eqn.3). The standard deviation is shown as the error bar on Figure 6 to represent the dispersion of the data around the averages' values.

$$SD = \sqrt{\frac{(x_1 - R)^2 + \cdots + (x_N - R)^N}{N}} \qquad (3)$$

© 2024 by ASME

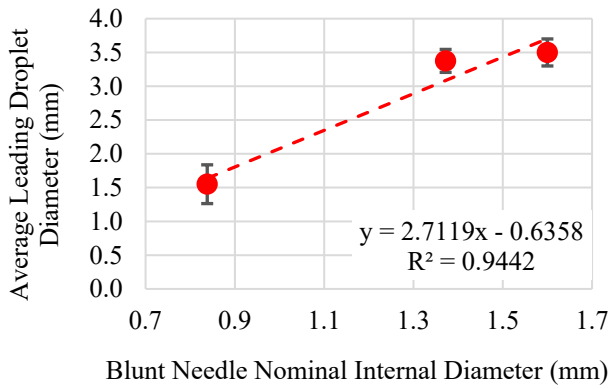

FIGURE 6: VARIATION OF AVERAGE LEADING DROPLETS DIAMETER VERSUS VARIATION OF NEEDLE SIZE.

The falling droplets are non-uniform in size and thus need to be grouped for data analysis, referred to as modes. Mode is defined as the most frequent number. In Figure 7 different modes for static droplets falling using 15 GA needle size at flow rate of 0.945 mL/s are shown. This figure indicates that most of the droplets are in mode 2 for this case. Note that the circle around the falling droplets serve as a reference only and are not the size of a droplet as defined by the software.

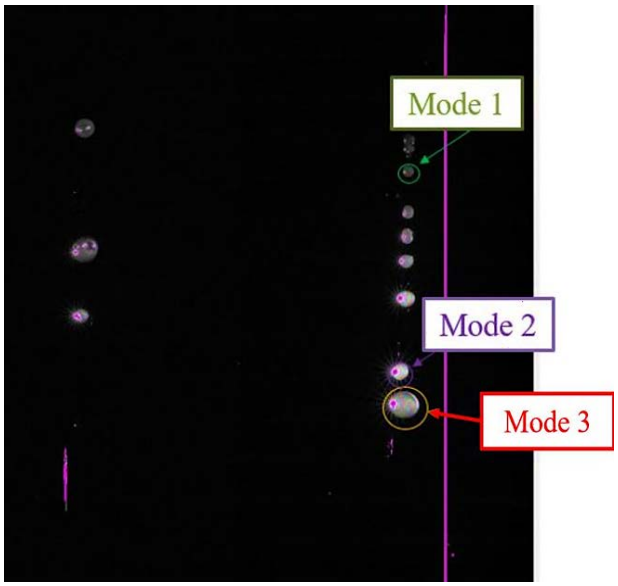

FIGURE 7: MODES OF DROPLETS FALLING FROM 15 GA NEEDLE AT 0.740 ML/S.

The changes in average velocity of water droplets in a single plane in terms of changes in flow rate for static and disturbed flow at different needle sizes are shown in Figure 8 and Figure 9, respectively. The results for the 14 GA, 15 GA, and 18 GA needle sizes indicate that the average velocity, diameter, and circularity for both static and disturbed flow is independent from flow rate. For disturbed and static flow using 18 GA needle size leads to the velocity increment up to 17.187% and 16.27%, respectively, by increasing the flow rate from 0.539 mL/s to 1.19 mL/s. However, average velocity indicates fluctuating variation by flow rate increment for 14 GA and 15 GA needle size. For static flow and using 15 GA needle size, the average velocity decreased 13.043% by increasing the flow rate from 0.539 mL/s to 1.19 mL/s. Also, for disturbed flow and same needle size of 15 GA, increasing flow rate from 0.539 mL/s to 0.74 mL/s leads to the decrement of 3.44%. But it is increased about 2.5% by increasing the flow rate up to 1.19 mL/s. Overall, by using the 18 GA needle size the average velocity has the maximum amount of 1.5 m/s at flow rate of 1.19 mL/s for both static and disturbed flow. The standard deviations are shown as the error bar on Figure 8 and Figure 9 to represent the dispersion of the data around the mean values.

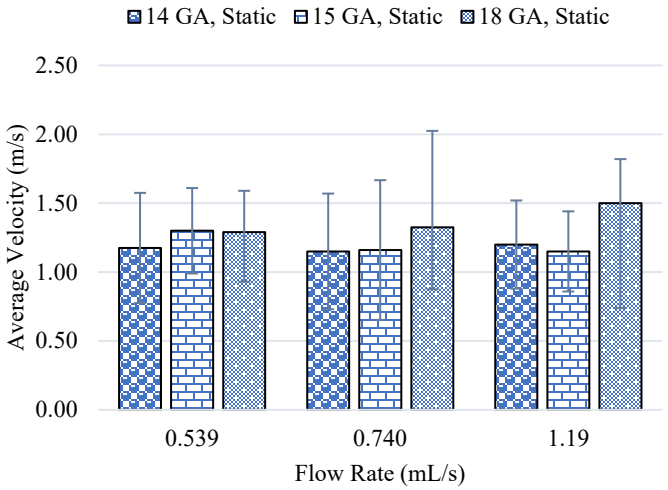

FIGURE 8: AVERAGE VELOCITY IN TERMS OF FLOW RATE FOR STATIC FLOW AT DIFFERENT NEEDLE SIZES.

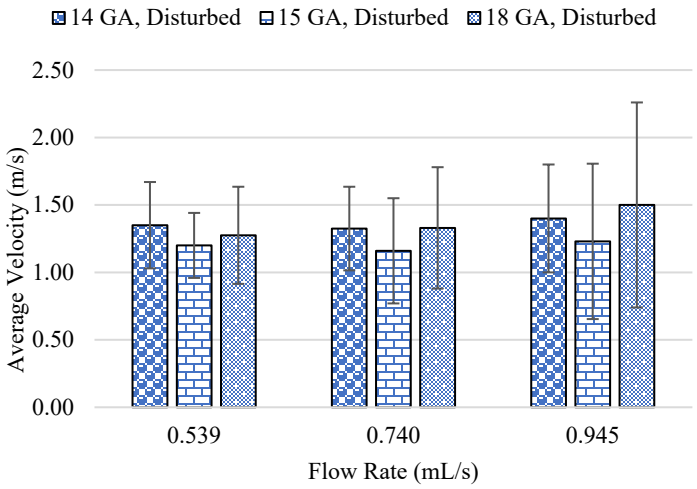

FIGURE 9: AVERAGE VELOCITY IN TERMS OF FLOW RATE FOR DISTURBED FLOW AT DIFFERENT NEEDLE SIZES.

© 2024 by ASME

For data analysis the average is calculated by combining the results of the specified needle at various flowrates (Fig. 10 and Fig. 11). Figure 10 shows the droplets' diameter for both static and disturbed flow in three modes. The maximum diameter of 3.5 mm is obtained by using 14 GA needle size. Also, using 14 GA and 15 GA needle size generates the maximum diameter of 3.4 mm for disturbed flow. Circularity can be defined by (Eqn.4) [14] where A and P are the area and perimeter of the 2D droplet image respectively. A circularity value of 1 and more than 1 is evident of circular and "non-circular" shapes, respectively. For other shapes such as an equilateral triangular, square, and hexagon, the circularity value is 0.605, 0.785, and 0.907, respectively. Some data points do not have three modes because minimum particle size was too high for the experiment run.

$$Circularity = \frac{4\,\pi\,A}{P^2} \qquad (4)$$

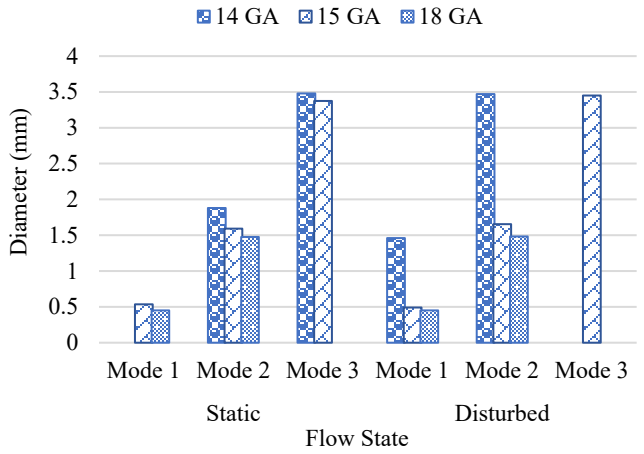

FIGURE 10: DROPLETS' DIAMETER VARIATION AT AVERAGED VARIOUS FLOWRATES AND DIFFERENT NEEDLE SIZES.

Water droplets in static condition are perfectly circular, however, non-circular shapes are being seen for disturbed flow. Figure 11 shows the non-circular shape of droplets using 18 GA needle size at flow rate of 0.740 mL/s. Hypothesis is that particles are affected by wind flow and particles colliding. To have a better understanding of the impact of flow type on droplets' properties, the disturbed and static results have been compared and shown in Figure 12.

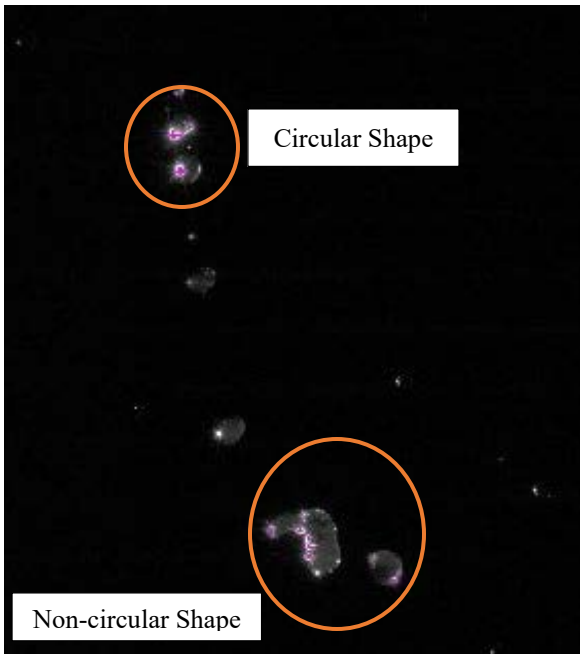

FIGURE 11: CIRCULAR AND NON-CIRCULAR SHAPE OF DROPLETS WHILE USING 18 GA NEEDLE SIZE AT FLOW RATE OF 0.740 ML/S IN DISTURBED FLOW.

Figure 12-A, shows the velocity, circularity, and droplets' diameter for static and disturbed flow by using 14 GA needle. By using this needle size, the maximum diameter is obtained as 3.50 mm for static flow. The average velocity is 15.25 % higher for disturbed flow. Figure 12-B demonstrates the droplets properties by using the 15 GA needle. For this needle size, droplets diameter is larger for disturbed flow and is 1.65 mm. The average velocity is 1.197 m/s and 1.203 m/s for disturbed and static flow, respectively. The comparisons between static and disturbed results for 18 GA needle size is shown in Figure 12-C. Based on the results, the blower has made droplets with larger diameter in compared to static. Also, the droplets shape is non-circular for disturbed flow with the circularity value greater than one. The average velocity for both static and disturbed flow types are 1.372 m/s and 1.368 m/s, respectively, which are similar. Generally, the average velocity at the average flow rate for both static and disturbed flow type using 15 GA are 1.20 m/s, 1.197 m/s, and for 18 GA are 1.37 m/s and 1.36 m/s, respectively, which are similar, but the average velocity in disturbed flow compared to static is 15.25% higher when using 14 GA needle size. Also, for static flow, increasing the needle size from 18 GA to 14 GA leads to the average velocity decrement by 16.27% at the average flow rate.

© 2024 by ASME

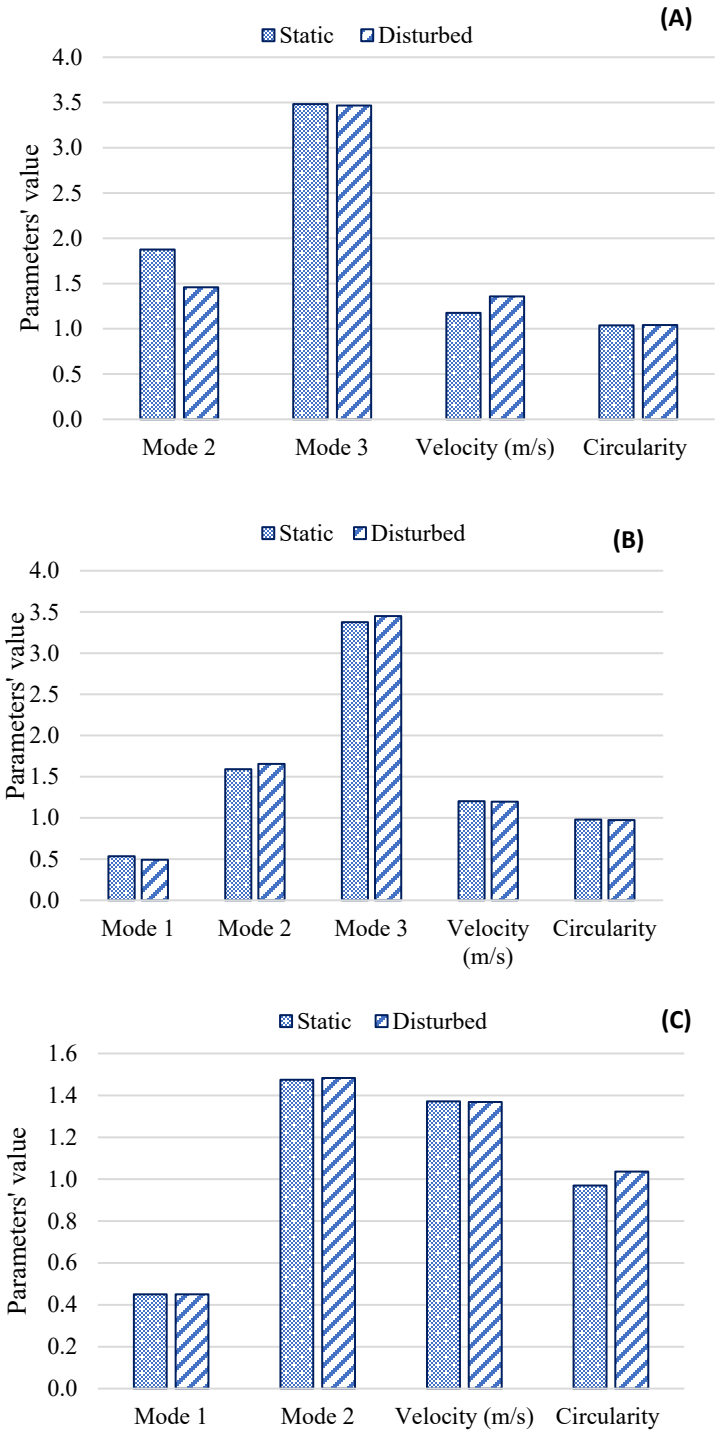

FIGURE 12: COMPARISON OF DISTURBED AND STATIC RESULTS WITH A) 14 GA NEEDLE SIZE, B) 15 GA NEEDLE SIZE, C) 18 GA NEEDLE SIZE.

4. CONCLUSION AND FUTURE WORK

Erosion generated by droplet impact on a solid surface is crucial in many pieces of industrial equipment, including wind turbines. This erosion reduces the effectiveness of the machine and incurs substantial maintenance costs. Testing the droplet erosion has been ongoing at the University of Tulsa but there was a need to quantify the falling droplets, which has been investigated in this work via PIV. The falling droplets were analyzed in a static field where the only force on the droplets was gravity as well as in a turbulent, disturbed field. This disturbed field was created with a small blower to create a uniform field of disturbance on the droplets formation and falling path. This turbulence simulates the deformation recorded within the erosion testing facility along with the measured wind speed due to the apparatus' rotation. PIV results have shown that the droplets vertical velocity remains constant between the static and disturbed fields with a minor velocity component in the horizontal plane with turbulence present. The droplets mean diameters, mode pattern, and circularity also showed no significant change between the two field settings. A truncation of the gathered data was noted for disturbed setting with smaller needle sizes, due to the droplets being blown out of the laser's 2D plane, so additional work is required. Future work will involve testing with more needle sizes to account for a wider range of droplet sizes in both static and disturbed field. Furthermore, a new method needs to be developed to investigate droplets moving out of the laser plane during disturbed flow and validate that the results include the droplets being affected by the disturbance. This work will aid in the erosion experimental facility's results as it translates the facility's settings into quantifiable values for modeling.

ACKNOWLEDGEMENTS

The authors would like to acknowledge the NSF REU Grant number 1852477 and Dr. Laura Ford for supporting the undergraduate student Emmelia Lichty to join this work.

REFERENCES

[1] Hoksbergen, T.H., Akkerman, R. and Baran, I., "Liquid droplet impact pressure on (elastic) solids for prediction of rain erosion loads on wind turbine blades," *Journal of Wind Engineering and Industrial Aerodynamics*, 233, p.105319, 2023.

[2] Liu, L., Zhang, Y., Cai, G. and Tsai, P.A., "High-speed dynamics and temperature variation during drop impact on a heated surface." International Journal of Heat and Mass Transfer 189, 122710, 2022.

[3] Marzbali, M. and Dolatabadi, A., "High-speed droplet impingement on dry and wetted substrates," *Physics of Fluids,* vol. 32, no. 11, 2020.

[4] Cimpeanu, R. and Papageorgiou, D.T., "Three-dimensional high speed drop impact onto solid surfaces at arbitrary angles," *International Journal of Multiphase Flow,* vol. 107, pp. 192-207, 2018/10/01/ 2018.

[5] Tang, C., Qin, M., Weng, X., Zhang, X., Zhang, P., Li, J. and Huang, Z., "Dynamics of droplet impact on solid surface with different roughness," *International Journal of Multiphase Flow,* vol. 96, pp. 56-69, 2017/11/01/ 2017.

© 2024 by ASME

[6] Haller, K.K., Ventikos, Y., Poulikakos, D. and Monkewitz, P., "Computational study of high-speed liquid droplet impact," *Journal of Applied Physics,* vol. 92, no. 5, pp. 2821-2828, 2002.

[7] Lesser, M.B., "Analytic solution of liquid-drop impact problems," *Proceedings of the Royal Society of London. A. Mathematical and Physical Sciences,* 377(1770), pp.289-308, 1981.

[8] Hancox, N. L., and J. H. Brunton. "A discussion on deformation of solids by the impact of liquids, and its relation to rain damage in aircraft and missiles, to blade erosion in steam turbines, and to cavitation erosion-The erosion of solids by the repeated impact of liquid drops." *Philosophical Transactions of the Royal Society of London. Series A, Mathematical and Physical Sciences* 260, no. 1110, 121-139, 1966.

[9] Fujisawa, N., Komatsu, M. and Yamagata, T., "Experimental study on erosion initiation via liquid droplet impingement on smooth and rough walls," *Wear*, 452, p.203316, 2020.

[10] Ahmad, M., Casey, M. and Sürken, N., 2009. Experimental assessment of droplet impact erosion resistance of steam turbine blade materials. *Wear*, 267(9-10), pp.1605-1618.

[11] Anderson, K., Karimi, S., and Shirazi, S., "Development of Droplet Erosion Testing Facility," Fluid Eng. Div., pp. 1-6, 2022.

[12] Ahmad, M., Schatz, M., Casey, M.V., "Experimental investigation of droplet size influence on low pressure steam turbine blade erosion," *Wear,* vol. 303, pp. 83-86, 2013.

[13] Kavian, A. *et al.*, "Simulated raindrop's characteristic measurements. A new approach of image processing tested under laboratory rainfall simulation," *Catena*, vol. 167, pp. 190-197, 2018.

[14] Cox, E. P. "A method of assigning numerical and percentage values to the degree of roundness of sand grains." *Journal of Paleontology,* 1, no. 3, 179-183, 1972.

© 2024 by ASME